Damage Mitigation of Conventional RC Shear Walls in High Seismic Zones

Emad A. Abraik[1], Maged A. Youssef[1], Salah F. El-Fitiany[1,2]

[1] Department of Civil and Environmental Engineering, Western University - London, ON, Canada.
[2] Structural Engineering Department, Alexandria University - Alexandria, Egypt.

ABSTRACT

Reinforced concrete (RC) walls constitute the main lateral load resisting system for the majority of buildings. Their inelastic response allows dissipating the seismic energy. This behaviour ensures achieving the life safety performance level on the cost of inducing significant damage to the buildings. The effect of using Engineering Cementitious Composite (ECC) and Superelastic Shape Memory Alloy (SE-SMA) on the seismic damage and ductility of RC walls is examined in this paper. Seismic fragility curves for convential steel RC walls and walls utilizing ECC and SE-SMA are developed for an assumed building. Results indicate that seismic damage in RC walls can be significantly reduced by utilizing ECC and/or SE-SMA.

Keywords: Shear wall, superelastic shape memory alloy, engineering cementitious composite.

INTRODUCTION

Reinforced Concrete (RC) shear walls are used to resist lateral loads due to their relatively high strength and stiffness. Seismic design codes aim at protecting the life of building occupants during major earthquakes. Meeting this objective requires reducing the risk of structural collapse and mitigating the structural damage.

Assessment of structural damage of conventional steel RC walls, after the 1964 Alaska earthquake, 2010 Chile Maule earthquake, and the 2011 New Zealand Christchurch earthquake showed that cases of significant damage and collapse have occurred. The global damage of RC shear walls can be correlated to the seismic-residual drift. A residual-drift ratio higher than 0.5% is considered the limit for repairable damage [1].

During the past decades, research efforts have focused on the development of self-centering seismic resisting systems that limit the seismic-residual drifts to an acceptable level. One possible system involves the use of superelastic (SE) shape memory alloy (SMA) material, which can undergo large strains, and recover them upon unloading by following a flagged-shape hysteresis [2]. The researched SE-SMA seismic resisting elements include vertical braces [3], base isolators [4], and dampers [5]. Several researchers investigated the use of SE-SMA bars to reinforce concrete elements including: beams [6], bridge columns [7], and shear walls [6]. Abdulridha [6] experimentally showed that the residual displacement of SE-SMA walls is about 15% less than that of steel RC walls. Abraik and Youssef [8, 9] concluded that the locations of SE-SMA bars in RC walls significantly affect the wall residual displacement. Abraik and Youssef [10] assessed the collapse vulnerability of SE-SMA RC shear walls and showed that SE-SMA RC walls exhibited lower seismic damage as compared to steel RC walls. Although there is a high potential for using SE-SMA in concrete structures, their use is still limited due to their low initial stiffness and their cost.

Replacing conventional concrete with Engineered Cementitious Composite (ECC) can significantly improve the ductility, bond strength, and mitigate the cracks. ECC materials possess a high tensile strain hardening of 4% [11], improved strength, ductility, and energy dissipation as compared to conventional concrete [12, 13]. Response of ECC RC beams [14] and columns [15] was found to be superior to that of conventional RC elements.

The aim of this paper is to evaluate the seismic performance of shear walls utilizing SE-SMA and/or ECC as compared to the conventional steel RC walls. A case study building is assumed, and its seismic performance is evaluated assuming different shear wall designs.

Numerical modeling

Modeling and nonlinear time history analyses are conducted using the Open System for Earthquake Engineering Simulation finite element software [16]. The walls are modeled using distributed-plasticity fiber-section elements. These elements account for moment-axial force interaction at each analysis step. The Menegotto-Pinto [17] and Mander et al. [18] uniaxial material constitutive models are used for steel reinforcement and the conventional concrete (confined and unconfined), respectively. The self-centering material model, shown in Figure 1a, is used to model the SE-SMA bars [19]. The assigned mechanical properties are taken from the experimentally-obtained values by Abdulridh [6] as summarized in Table 1. Figure 1b shows the constitutive stress-strain relationship for the ECC material [13]. The input parameters for the ECC material are summarized in Table 2. The effect of confinement on the mechanical properties of the ECC is implemented in the numerical model following the recommendations of Motaref et al. [20].

Table 1. SE-SMA material properties.

Model Parameter	Value
Austenite yield strength, f_{SMA} (MPa)	380
Austenite modulus, K_1 (MPa)	36459
Post-yield stiffness, K_2 (MPa)	365
Lower plateau stress factor	0.55
Recoverable strain	7.0%

Table 2. ECC material properties.

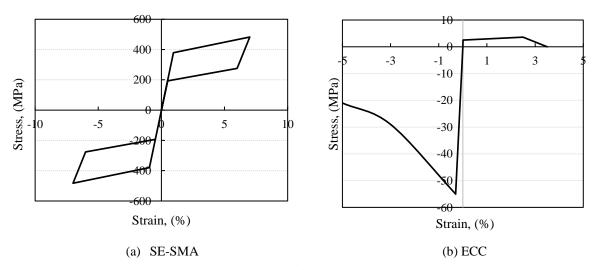| Model Parameter	Value
Young's modulus, E (MPa)	25000
Compressive strength, (MPa)	55
Strain at peak compressive strength	0.003
First cracking strain, ε_{t0}	0.0001
Tensile strength (MPa)	3.60
Strain at peak tensile strength	0.025
Tensile strain capacity	0.035

(a) SE-SMA

(b) ECC

Figure 1. Utilized material models

Assessment Criteria

Two strain limits are used to assess the serviceability and damage control phases as recommended by Kowalasky [21]. The serviceability strain limit reflects a minimum post-seismic damage. The damage control strain reflects extensive repairable seismic damage. The serviceability and damage control strain limits are taken equal to 0.004 and 0.018 for unconfined and confined concrete in-compression [21], and 0.015 and 0.060 for steel bars [21]. The serviceability limit is not needed for SE-

SMA nor ECC as the material is assumed to functioning until the damage limit. The damage strain limit is taken equal to 0.07 for SE-SMA [22], 0.0400 for ECC in-compression [23], and 0.0025 for ECC in-tension [23].

Modeling Validation

Abdulridh [6] performed large-scale tests on concrete shear walls reinforced with SE-SMA bars. Characteristics of the tested specimens are listed in Table 3. Figure 2 shows a comparison between the numerical model and the experimental test results. The numerical model has accurately captured the overall response of the experimental test.

Table 3. SE-SMA RC wall design details.

Wall ID	h_w (mm)	L_w (mm)	T (mm)	f_c' (MPa)	f_y (MPa)	ρ_{vb} (%)	$\rho_v = \rho_h$ (%)
SE-SMA	2200	1000	150	30	400	1.68	1.88

Where L_w is the wall length, h_w is the wall height, T is the wall thickness, f_c' is the concrete compression strength, f_y is the steel yield strength, ρ_{vb} is the vertical steel ratio at the boundary elements, ρ_v is the vertical at the web, and ρ_h is the horizontal steel ratio.
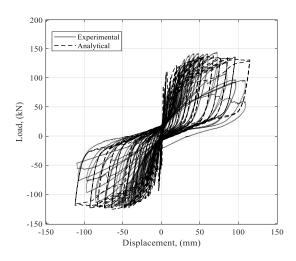

Figure 2. Load-displacement results of SE-SMA RC wall

Case Study Building

A 10-story office building was assumed to be located in Vancouver, BC. The building has a footprint of 12 m by 12 m and a typical story height of 2.8 m. The assumed soil profile is class D with a shear wave velocity ranging between 180 and 360 m/s. The lateral force resistance system consists of RC shear walls, as shown in Figure 3a. The seismic lumped masses were calculated considering gravity loads plus 25% of the live load (2.8 kPa) as per NBCC [24].

The walls were first designed as conventional steel RC walls using the Equivalent Lateral Force Method assuming a design force reduction factor *R* of 5.6. The shear wall design and reinforcement are shown in Figure 3b. A second design is assumed by replacing the concrete with ECC. In the third design, SE-SMA bars replaced the steel bards in the boundary elements for the plastic hinge length. Steel bars are assumed to be connected to the SE-SMA bars using mechanical couplers. The plastic hinge length (L_P) is calculated using equation (1), stipulated in CSA A23.3-14 [25]. Eigenvalue analysis is carried out to determine the first (T_1) and second (T_2) elastic periods, shown in Table 4. The periods of the three walls were almost equal.
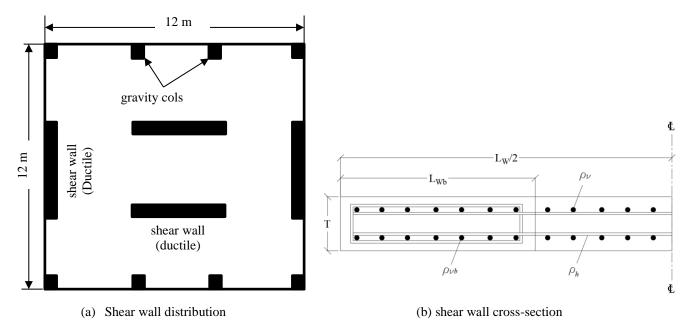
$$L_P = 0.5\ L_w + 0.1\ h_w \tag{1}$$

(a) Shear wall distribution   (b) shear wall cross-section

Figure 3. Studied building geometry and wall reinforcement

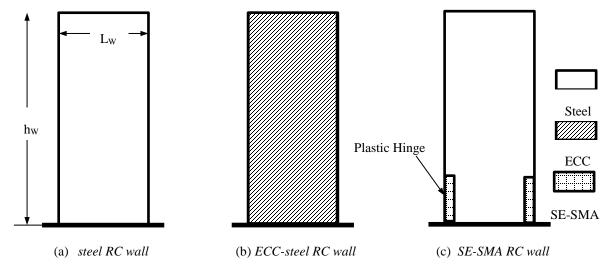(a) *steel RC wall*   (b) *ECC-steel RC wall*   (c) *SE-SMA RC wall*

Figure 4. Vertical reinforcement types and distribution

Table 4. First and second period for each wall.

Model Parameter	Steel RC wall	ECC-steel RC wall	SE-SMA RC wall
T_1	1.70	1.76	1.71
T_2	0.28	0.33	0.33

Ground Motion Records

Twenty ground motions are extracted from the PEER ground motion database and are listed in Table 5. The selected ground motions are scaled to the level of the mean design spectrum over a period ranging from 0.2 T_2 to 1.5 T_1 using the Mean Square Error (MSE).

Table 5. Summary of selected ground motions.

Ground Motion	Station	Magnitude	Scale Factor
Imperial Valley-06	Calipatria Fire Station	6.53	3.67
Imperial Valley-06	Delta	6.53	1.08
Imperial Valley-06	El Centro Array #1	6.53	3.02
Imperial Valley-06	El Centro Array #12	6.53	1.96
Imperial Valley-06	El Centro Array #13	6.53	2.64
Imperial Valley-06	Parachute Test Site	6.53	2.69
Superstition Hills-02	Westmorland Fire Sta	6.54	1.49
Loma Prieta	Agnews State Hospital	6.93	1.85
Northridge-01	LA - Baldwin Hills	6.69	1.78
Northridge-01	LA - W 15th St	6.69	2.47
Chuetsu-oki, Japan	Hinodecho Yoshida Tsubame City	6.80	2.18
Chuetsu-oki, Japan	Niigata Nishi Kaba District	6.80	1.89
El Mayor-Cucapah, Mexico	Michoacan De Ocampo	7.20	0.61
El Mayor-Cucapah, Mexico	Calexico Fire Station	7.20	1.25
Darfield, New Zealand	DFHS	7.00	1.10
Darfield, New Zealand	Pages Road Pumping Station	7.00	1.42
Darfield, New Zealand	Riccarton High School	7.00	1.50
Darfield, New Zealand	SBRC	7.00	2.60
Darfield, New Zealand	Styx Mill Transfer Station	7.00	1.54
El Mayor-Cucapah, Mexico	Westside Elementary School	7.20	1.10

Seismic Response

Figure 5a shows the envelopes for the mean inter-story drift ratios for the considered walls. As shown in the figure, the lower stiffness of the SE-SMA material results in a 22% increase of the top inter-story drift ratio. The difference in the mean inter-story drift ratios between the steel RC and the ECC-steel RC walls is negligible. However, using SE-SMA bars reduces the mean residual inter-story drift ratios by 28% on average as compared to the steel RC wall, as shown in Figure 5b. The ECC-steel RC wall exhibits a 33% increase in its mean residual inter-story drifts.
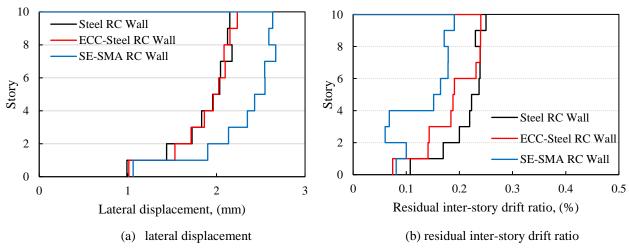

(a) lateral displacement   (b) residual inter-story drift ratio

Figure 5. Seismic analysis results

Collapse Risk Assessment

The disaggregation of annual probability of collapse risk assessment (λ_c) is used to identify the contribution of different levels of ground motion intensity to the total collapse. Two components are needed to calculate λ_c: the seismic hazard curve and the structural collapse fragility curve. The seismic hazard curve represents the mean annual probability of exceeding the considered ground motion intensity at the building location, while the structural collapse fragility curve determines the probability of structural collapse for each ground motion intensity $S_a(T_1, 5\%)$. λ_c is calculated by integrating the structure collapse fragility curve over the seismic hazard curve using Equation (2) [26].

$$\lambda_c = \int_0^\infty P(C \backslash Sa) . \left| \frac{d\lambda_{sa}(Sa)}{d(Sa)} \right| . d(Sa) \tag{2}$$

Where $\frac{d\lambda_{sa}(Sa)}{d(Sa)}$ is the slope of the seismic hazard curve, and $P(C \backslash Sa)$ is the probability that the structure will collapse when subjected to a given earthquake ground motion.

The seismic hazard curves for Vancouver, BC, are shown in Figure 6. Figures 7 and 8 provide the fragility curves and the collapse risk curves, respectively. λ_c per year is 9.09×10^{-4}, 1.31×10^{-4}, and 1×10^{-4} for steel RC wall, SE-SMA RC wall, and steel ECC RC wall, respectively. These values are converted using EQ (3) to 4.44%, 0.65%, and 0.94%, considering 50 years exceedance period.

$$P_c(\text{in } t \text{ years}) = 1 - e^{-\lambda_c t} \tag{3}$$

The risk of collapse of the ECC RC and the SE-SMA RC walls is less than the steel RC wall. The maximum risk of collapse, as shown in Figure 8, occurs at 0.2g, 0.3g, and 0.4g for steel RC wall, ECC RC wall, and SE-SMA RC wall, respectively, which are associated with a probability of collapse of 30%, 39%, and 64% (Figure 7). Although the SE-SMA RC wall exhibits a higher probability of collapse, the value occurs at 0.4g which is 100% higher than the steel RC wall. For fair comparison, FEMA P695 [27] defines the collapse probability at 50% as the median collapse capacity ($\hat{S}_{CT}$). The $\hat{S}_{CT}$ value is 91%, 63%, and 78% for steel RC wall, ECC RC wall, and SE-SMA RC wall, respectively.
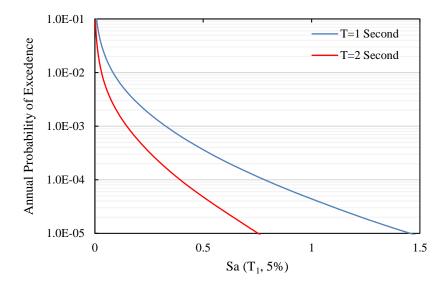

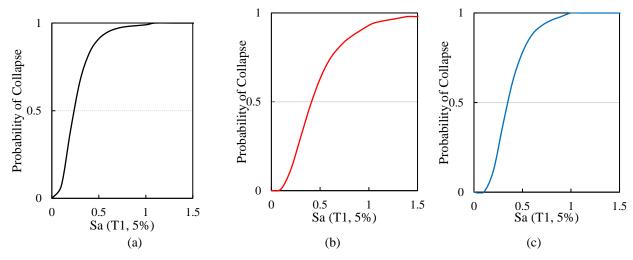*Figure 6. Seismic hazard curve for Vancouver, BC (location 49.233, -123.15)*

Figure 7. Seismic fragility curves: (a) steel RC wall; (b) ECC-steel RC wall; (c) SE-SMA RC wall
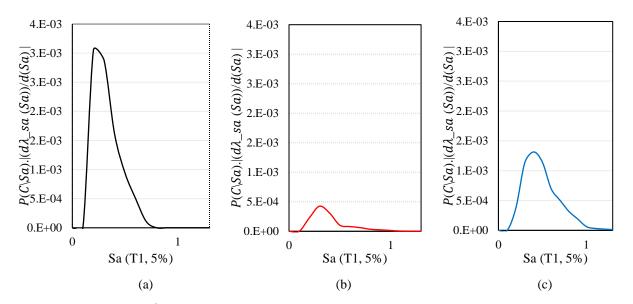

Figure 8. λ_c curve: (a) steel RC wall; (b) ECC-steel RC wall; (c) SE-SMA RC wall

CONCLUSIONS

Hypothetical a ten-story building located on Vancouver, BC on-site class D was designed according to NBCC, 2015 [24]. Nonlinear time history analysis was then carried out. Based on the findings of this study, the following conclusions and recommendations are obtained:

1. The difference in inter-story drift ratio between the steel RC wall and the ECC-RC wall is negligible.
2. The SE-SMA RC wall has the highest inter-story drifts and the lowest residual inter-story drift. The use of SE-SMA bars mitigates the residual inter-story drift ratio due to their flag-shape response as compared to the typical hysteretic curve of steel RC wall and the ECC-steel RC wall.
3. At 50% probability of collapse, the steel RC wall exhibits a high probability of collapse (91%) as compared to 63% and 78% for ECC-steel RC wall and SE-SMA RC wall, respectively.
4. The predicted annual probability of collapse of steel RC wall is 9.09×10^{-4} which is associated with a probability of collapse of only 39%. For the ECC-steel RC wall and SE-SMA RC wall, the λ_c values are corresponding to a probability of collapse is 30% and 64%, respectively.

REFERENCES

[1] McCormick, J., Tyber, J., DesRoches, R., Gall, K., & Maier, H. (2008). "Permissible residual deformation level for building structures considering both safety and human elements". *Proceedings of the 14th World Conference on Earthquake Engineering, Beijing, China*.

[2] McCormick, J., Tyber, J., DesRoches, R., Gall, K., & Maier, H. (2007). "Structural engineering with NiTi. II: mechanical behavior and scaling." In *ASCE 10th Structures Congress*, San Antonio, TX, USA.

[3] Araki, Y., Shrestha, K., Maekawa, N., Koetaka, Y., Omori, T., & Kainuma, R. (2016). "Shaking table tests of steel frame with superelastic Cu-Al-Mn SMA tension braces". *Earthq Eng Struct D, 45*(2), 297–314.

[4] Ozbulut, O., & Silwal, B. (2016). "Performance assessment of buildings isolated with S-FBI system under near fault earthquakes". *Smart Struct Syst, 17*(5), 709-724.

[5] Ma, H., & Cho, C. (2008). "Feasibility study on a superelastic SMA damper with re-centring capability". *A 473*(1-2), 290-296.

[6] Abdulridha, A. (2012). "Performance of superelastic shape memory alloy reinforced concrete elements subjected to monotonic and cyclic loading". Ottawa: Ph.D. Thesis: University of Ottawa.

[7] Tazarv, M., & Saiidi, M. (2013). "Analytical studies of the seismic performance of a full-scale SMA-reinforced bridge column". *International Journal of Bridge Engineering, 1*(1), 37-50.

[8] Abraik, E., & Youssef, M. (2015). "Cyclic performance of shape memory alloy reinforced concrete walls". *Response of structures under extreme loading* (pp. 326-333). Lansing, MI: The fifth international workshop on performance, protection, and strength of structures under extreme loading.

[9] Abraik, E., & Youssef, M. (2016). "Performance assessment of three-story shape memory alloy reinforced concrete walls". *CSCE 5th International Structural Specialty Conference*, *852*. London, ON, Canada.

[10] Abraik, E., & Youssef, M. (2018). "Seismic fragility assessment of superelastic shape memory alloy reinforced concrete shear walls". *Journal of building engineering, 19*, 142-153.

[11] Li, M., Luu, H. C., Wu, C., Mo, Y. L., & Hsu, T. T. (2014). "Seismic performance of reinforced engineered cementitious composite shear walls". *7*, 691-704.

[12] Hung, C., & El-Tawil, S. (2010). "Seismic Behavior of a Coupled-Wall System with Hpfrcc Coupling Beams". *Structures Congress* (pp. 1864-1873). Orlando, Florida, United States: American Society of Civil Engineers.

[13] Gencturk, B., Kaymaz, I., & Hosseini, F. (2016). "Derivation of Seismic Design Parameters for ECC and Multi-Material Special Moment-Resisting Frames". *Journal of Earthquake Engineering, 20*(7), 1054-1076.

[14] Yuan, F., Pan, J., Dong, L., & Leung, C. K. (2014). "Mechanical behaviors of steel reinforced ECC or ECC/concrete composite beams under reversed cyclic loading". *Journal of Material in Civil Engineering, 26*(8), 04014047.

[15] Wu, C., Pan, Z., Su, R., Leung, C., & Meng, S. (2017). "Seismic behavior of steel reinforced ECC columns under constant axial loading and reversed cyclic lateral loading". *Materials and Structures, 50*(78). doi:10.1617/s11527-016-0947-9.

[16] OpenSees. (2018). Open system for earthquake engineering simulation. Berkeley, CA.

[17] Menegotto, M., & Pinto, P. (1973). "Method of analysis of cyclically loaded RC plane frames including changes in geometry and non-elastic behavior of elements under normal force and bending". Preliminary Report ABSE, vol 13.

[18] Mander, J. B., & Priestley, M. J. (1988). "Theoretical stress-strain model for confined concrete". *Journal of Structural Engineering. ASCE, 114*(4), 1804-1826.

[19] Christopoulos, C., Tremblay, R., Kim, H.-J., & Lacerte, M. (2008). "Self-centering energy dissipative bracing system for the seismic resistance of structures: development and validation". *Journal of Structural Engineering ASCE, 134*(1), 96-107.

[20] Motaref, S., Saiidi, S., & Sanders, D. H. (2011). "*Seismic response of precast bridge columns with energy dissipating joints*". Reno, NV: Rep. No. Center for Civil Engineering Earthquake Research Dept. of Civil and Environmental Engineering, Univ. of Nevada, Reno, NV.

[21] Kowalsky, M. J. (2000). "Deformation limit states for circular reinforced concrete bridge columns". *J Struct Eng, 126*(8), 869-878.

[22] Hurlebaus, S., & Gaul, L. (2006). "Smart structure dynamics. *Mechanical system and signal*, 255-281.

[23] Pan, J. L., & Yuan, F. (2013). "Experimental study on flexural behaviors of engineered cementitious composite beams reinforced with FRP bars". *International Conference on Fracture Mechanics of Concrete and Concrete Structures FraMCoS-8*, (pp. 1-11). Toledo.

[24] NBCC. (2015). *National Building Code of Canada.* National research council of Canada, Ottawa.

[25] Canadian Standard Association - CSA (2014). *CAN/CSA-A23.3:* Prepared by the CSA, Toronto, ON.

[26] Ugurhan, B., Baker, J. Deierlein, G. (2014). "Uncertainty estimation in seismic collapse assessment of modern reinforced concrete moment frame buildings". Anchorage, AL: Tenth U.S. National conference on earthquake engineering frontiers of earthquake engineering.

[27] FEMA (2009) Quantification of building seismic performance factors, federal emergency management agency. FEMA P695, Washington, DC.